Regional Striatal DOPA Transport and Decarboxylase Activity in Parkinson's Disease

Hiroto Kuwabara, Paul Cumming, Yoshifumi Yasuhara, Gabriel C. Léger, Mark Guttman, Mirko Diksic, Alan C. Evans and Albert Gjedde

McConnell Brain Imaging Center, Montreal, Canada; Montreal Neurological Institute, Montreal, Canada; and Department of Neurology and Neurosurgery, McGill University Faculty of Medicine, Montreal, Canada

Methods: We measured blood-brain barrier transport and decarboxylation of 6-[^{18}F]fluoro-L-DOPA (FDOPA) using PET in patients with Parkinson's disease (n = 7, 57 ± 7 yr) and age-matched control subjects (n = 7, 60 ± 6 yr). To visually present regional changes of FDOPA uptake in Parkinson's disease, we introduced maps of FDOPA uptake relative to occipital cortex, averaged across control subjects and Parkinson's disease patients in an MRI-based stereotaxic coordinate space. **Results:** There was no significant changes in the blood-to-brain transport of FDOPA (K_1^D) in Parkinson's disease. The K_1^D values of the head of caudate were lower than those of putamen in both normal subjects and Parkinson's disease patients. In Parkinson's disease, the activity of L-DOPA decarboxylase (DDC) was differentially reduced in subdivisions of striatum. The residual DDC activity was 63% of the control value in the head of caudate nucleus, 54% in the anterior putamen and 39% in the posterior putamen. The DDC activity in frontal and occipital cortices remained unchanged by the disease. Subtraction of averaged FDOPA uptake maps (control minus Parkinson's disease) visualized a spatial pattern of pathological changes in FDOPA uptake common to Parkinson's disease patients. **Conclusion:** The striatal blood-to-brain transport of FDOPA remained unchanged while the DDC activity was differentially reduced within the striatum in Parkinson's disease. We found the FDOPA uptake maps useful in identifying altered patterns of FDOPA metabolism common in Parkinson's disease.

Key Words: Parkinson's disease; striatum; L-dopa decarboxylase; blood-to-brain transport; functional maps

J Nucl Med 1995; 36:1226-1231

I t has been demonstrated that 6-[^{18}F]fluoro-L-DOPA (FDOPA) and PET are useful in monitoring presynaptic dopaminergic neurotransmission in the human brain (*1–3*). FDOPA-PET studies are commonly analyzed by graphical analyses for estimates of the net clearance rate constant of FDOPA into the brain, often collectively referred to as the uptake constant of FDOPA (*4–8*). In Parkinson's disease,

the uptake constant correlates with the clinical stage of the disease and aids differentiation from other movement disorders, including multiple system atrophy and progressive supranuclear palsy (*7,9,10*). Within the striatum of Parkinson's disease patients, the uptake constant is lower in putamen, especially in the posterior part than in the head of the caudate nucleus (*7,11*).

The uptake constant of FDOPA, however, represents the combined effects of the two key steps of FDOPA kinetics; the transport of FDOPA across the blood-brain barrier (BBB) and decarboxylation of FDOPA by L-dopa decarboxylase (E.C. 4.1.1.26) (DDC) (*9,12*). Separate measurements of these steps are important in Parkinson's disease for several reasons. First, pathological changes of the blood-to-brain transport in Parkinson's disease are not well documented, although the delivery of exogenous levodopa, the major therapy for the disease, entirely depends on this facilitated transport. Recently, Alexander et al. reported significant reduction of the blood-to-brain transport of levodopa in MPTP parkinsonian monkeys (*13*). Second, despite discontinuation of therapeutic levodopa prior to PET studies, the major plasma metabolite, O-methyl-L-dopa, may persist in plasma due to a longer plasma half-life, and interfere with FDOPA transport (*14*).

In the present study, we present estimates of the blood-to-brain transfer (K_1^D) and the relative activity of DDC (k_3^D) in patients suffering from Parkinson's disease. To emphasize a pattern of regional neurochemical pathology of the striatum in Parkinson's disease, we grossly subdivided the striatum into the head of caudate nucleus, and the anterior and posterior portions of putamen.

Visualization and recognition of the spatial pattern of FDOPA uptake by means of pixel-by-pixel images is intended to facilitate clinical diagnosis. Parametric images of K_1^D and k_3^D are not currently available due to the statistical noise of measurements made with PET. For this reason, we extend the concept of so-called "striato-occipital ratio" to "pixel-occipital ratio" images to extract combined effects of Parkinson's disease on the blood-to-brain transport and DDC activity. Analogous to the techniques used in the functional mapping of the brain, images are transformed to an MRI-based stereotaxic coordinate space, averaged across control subjects and Parkinson's disease patients

and subtracted to elucidate changes common to Parkinson's disease (15,16).

MATERIALS AND METHODS

Patients and Subjects

We studied seven patients with Parkinson's disease (age: 57 ± 7 yr) and seven healthy, neurologically normal volunteers (60 ± 6 yr). All subjects gave written, informed consent to the study, previously approved by the Ethics and Research Review Committee of the Montreal Neurological Institute. The normal subjects were recruited from the general public and screened for past and present medical and psychiatric histories, including substance abuse. The patients were seen by a neurologist (MG). The patients suffered locomotor disability on Stages 3-4 of the Hoehn and Yahr scale onset within 3-5 yr at the time of PET study (17). Patients were treated with 400-1100 mg levodopa per day. Three patients received bromocriptine and one deprenyl in addition to levodopa, while the remaining three patients recieved levodopa-carbidopa alone. All medications were interrupted at least 12 hr prior to the PET study. All subjects were fasted overnight and pretreated with 100 mg carbidopa approximately 90 min before the PET study.

PET Procedures

Subjects reclined on a couch and head movement was lightly restrained with a custom-made head holder of rapidly setting foam. Thin catheters (20-g Cathlon IV) were placed in a brachial artery for blood sampling and an antecubital vein for tracer injection. The study room was dimly lit, quiet and maintained at 20-23°C.

During 90 min after intravenous administration of 200 MBq of FDOPA, we recorded the radioactivity in the brain with the Scanditronix PC2048 15B (Upsala, Sweden) PET camera. The PET camera has an in-plane resolution of 5.8-6.4 mm and an axial resolution of 6.1-7.1 mm FWHM with 15 simultaneous planes (18). The frame schedule was six 30-sec frames followed by seven 1-min, five 2-min, four 5-min and five 10-min frames. Arterial blood samples were taken every 10 sec in the beginning and at increasing intervals toward the end of the study. Following centrifugation, radioactivity in arterial plasma was determined with the Canberra 802-3W well-type scintillation spectrometer (Ramsey, NJ) cross-calibrated with the PET camera and corrected for the plasma volume. Plasma samples taken at 2.5, 5, 10, 15, 20, 25, 30, 35, 45 and 60 min were fractionated by high-performance liquid chromatography (HPLC) with one-line gamma detection (Berthold LB 507A) to separate radioactive species in plasma (19). We found FDOPA and 3-O-methyl-6-[^{18}F]fluorodopa (OMFD) to be the major plasma radioactivity sources. Minor plasma metabolites, including sulfo-conjugates of 6-[^{18}F]fluorodopamine (< 5%), were assumed not to enter the brain. Prior to the FDOPA study, tissue attenuation was determined with a 511-keV gamma source (^{68}Ga). Each PET frame was reconstructed to a 128 × 128 matrix of 2 × 2 mm pixels (25.6 mm^3 in volume), correcting for tissue attenuation, deadtime, scatter and coincident counts.

On a separate occasion, we obtained 64 2-mm thick axial T2-weighted MR images. The MRI volume was co-registered with a three-dimensional PET transmission volume and MR images were re-sampled to the plane of PET images (20). We identified and outlined the frontal and occipital cortices, head of caudate nucleus and putamen on matched MR images, thus obtaining the individual's template of regions of interest (ROIs). The putamen was subdivided into anterior and posterior halves. The occipital ROIs were used to construct pixel-to-occipital radioactivity ratio images. We identified the three striatal structures in at least four consecutive matched MRI planes and used the middle two planes for analysis. The time courses of radioactivity in these structures were obtained by applying the stored ROI templates to successive PET frames, and weighted averages for the above structures were obtained. We treated the left and right sides of striatal subdivisions separately on the grounds that Parkinson's disease may have asymmetric pathology. For the cortical regions, the radioactivity time courses were weighted averaged for the two sides.

Data Analysis

In the frontal cortex, we estimated the unidirectional blood-to-brain clearance (K_1^D), the partition volume ($V_e = K_1/k_2$, where k_2 is the fractional brain-to-blood clearance), the relative DDC activity (k_3^D) and the effective vascular volume (V_0), using radioactivity time courses in brain and plasma recorded during the first 60 min following tracer injection. We constrained the ratio of the unidirectional blood-to-brain clearances of FDOPA and OMFD to 2.3 (21). In the striatal subdivisions, we estimated only K_1^D, k_3^D and V_0, using data obtained during the first 40 min of the study. We constrained the partition volume to the estimates of the frontal cortex of individual subjects. The use of these biological constraints has been validated and discussed in detail elsewhere (22,23).

Averaged Images

We normalized the radioactivity of each pixel to the average occipital radioactivity between 60 and 90 min. The ratio images were transformed to a common stereotaxic coordinate space based on the atlas of Talairach and Tournoux (24) but re-scaled so that the length of the transverse and sagittal axes were equal (15). These transformed images were averaged across subjects of the same clinical category (i.e., control subjects and Parkinson's disease patients) (16). The averaged patient and control images were subtracted (control minus Parkinson's disease), and normalized to the control image, to yield change distribution images. The above functional images could be merged with the averaged MR image with color display. We presented images in a gray scale with superimposed grids to aid MR-PET correlation. All images were taken from the transverse section of the brain parallel to and 3.7 mm above the AC-PC plane, the transverse plane passing through the anterior and posterior commissures.

Statistical Methods

Results were expressed as means and standard deviations. We used Student's t-tests to compare means and paired t-tests to compare the same variable in different structures (including subdivisions) within the same clinical categories (Parkinson's disease patients or control subjects). The null hypothesis (equal means) was rejected at or less than the 0.05 level. The p values were corrected for multiple comparisons according to the Bonferroni procedure (25).

RESULTS

The areas of striatal subdivisions identified on matched MR images were 1.44 ± 0.23 cm^2 for the caudate head, 1.82 ± 0.30 cm^2 for the anterior putamen and 1.56 ± 0.31 cm^2 for the posterior putamen in control subjects, and 1.52 ± 0.27 cm^2, 1.78 ± 0.39 cm^2 and 1.55 ± 0.33 cm^2, respectively, in Parkinson's disease patients. There was no

TABLE 1
Unidirectional Blood-to-Brain Clearance of FDOPA (K_1^D)

Region	Control subjects ($ml\ g^{-1}\ min^{-1}$)	Parkinson's disease ($ml\ g^{-1}\ min^{-1}$)
Frontal cortex	0.031 ± 0.005	0.029 ± 0.007
Occipital cortex	0.039 ± 0.010	0.037 ± 0.010
Caudate head	0.032 ± 0.008	0.033 ± 0.008
Anterior putamen	0.042 ± 0.009*	0.040 ± 0.011*
Posterior putamen	0.046 ± 0.008*	0.041 ± 0.012*

*p < 0.05; caudate head vs. anterior or posterior putamen.

significant difference between areas of these striatal subdivisions of patients and controls.

The partition volume ($V_e = K_1/k_2$) averaged 0.69 ± 0.10 and 0.66 ± 0.12 ml g^{-1} in frontal and occipital cortices for control subjects and 0.66 ± 0.12 and 0.68 ± 0.13 ml g^{-1} for Parkinson's disease patients. We found no statistical difference between patients and controls.

Table 1 lists regional values of the unidirectional blood-to-brain clearance of FDOPA. In frontal and occipital cortices and striatal subdivisions, we found the K_1^D estimates of Parkinson's disease patients were not statistically different from those of control subjects. The anterior and posterior putamen K_1^D values were significantly greater than those of the caudate head in both control subjects and Parkinson's disease patients.

Table 2 lists regional values of the relative DDC activity. We found no significant changes in the k_3^D estimates between control subjects and Parkinson's disease patients in both frontal and occipital cortices. Among striatal subdivisions of control subjects, the k_3^D values were highest in the anterior putamen and lowest in the caudate head. We found no statistical differences among the k_3^D values of different striatal subdivisions in control subjects. In Parkinson's disease patients, the DDC activity was most preserved in the caudate head, and most severely impaired in the posterior putamen. The residual DDC activities in Parkinson's disease patients were 63% in the caudate head,

TABLE 2
Relative DDC Activity (k_3^D)

Region	Control subjects (min^{-1})	Parkinson's disease (min^{-1})
Frontal cortex	0.010 ± 0.002	0.009 ± 0.006
Occipital cortex	0.009 ± 0.001	0.007 ± 0.006
Caudate head	0.076 ± 0.022	0.048 ± 0.015*
Anterior putamen	0.080 ± 0.013	0.043 ± 0.011†
Posterior putamen	0.071 ± 0.012	0.028 ± 0.010†

*p < 0.0005; †p < 0.0001; control subjects vs. Parkinson's disease patients.
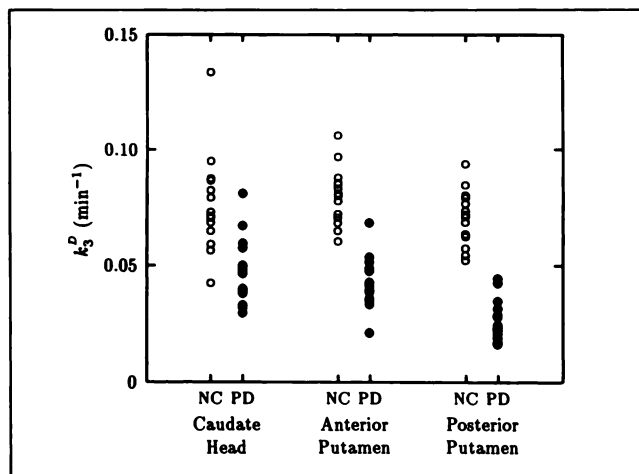
FIGURE 1. Plots of individual values of the relative activity of L-DOPA decarboxylase (k_3^D) for the caudate nucleus head and the anterior and posterior subdivisions of putamen. Open circles are the k_3^D values of normal subjects; closed circles are Parkinson's disease patients.

54% in the anterior putamen and 39% in the posterior putamen of corresponding control values. The k_3^D values of the posterior putamen were significantly lower than those of the caudate head and anterior putamen in Parkinson's disease patients.

Figure 1 plots individual k_3^D values in striatal subdivisions for which means and standard deviations were listed in Table 2. In the caudate head, 6 of 14 parkinsonian k_3^D values were lower than the lowest control k_3^D value (the left and right sides of striatal subdivisions were treated independently). In the anterior putamen, all but one of 14 parkinsonian values were lower than the lowest control value. In the posterior putamen, there was no overlap between parkinsonian and control values. There was no distinctive gap, however, between k_3^D values of Parkinson's disease and control subjects in any striatal subdivisions.

Figure 2 shows the normalized averaged pixel radioactivity images for control subjects (Fig. 2A) and for Parkinson's disease patients (Fig. 2B), the relative change image (Fig. 2C) and the averaged MR image (Fig. 2D) for a transverse section parallel to and 3.7 mm above the AC-PC plane. For control subjects (Fig. 2A), the radioactivity was specifically accumulated in the striatum, and the ratio was relatively uniform throughout the cortex with a slight frontal-to-occipital gradient. For Parkinson's disease patients (Fig. 2B), striatal accumulation of activity was limited to the caudate head and, to a lesser degree, to the anterior putamen. The relative change image (Fig. 2C: Fig. 2A minus Fig. 2B, normalized to Fig. 2A) confirmed that the pathological change was most evident in the posterior putamen of Parkinson's disease patients.

DISCUSSION

We demonstrated a differential reduction of the relative DDC activity in subdivisions of the striatum in Parkinson's
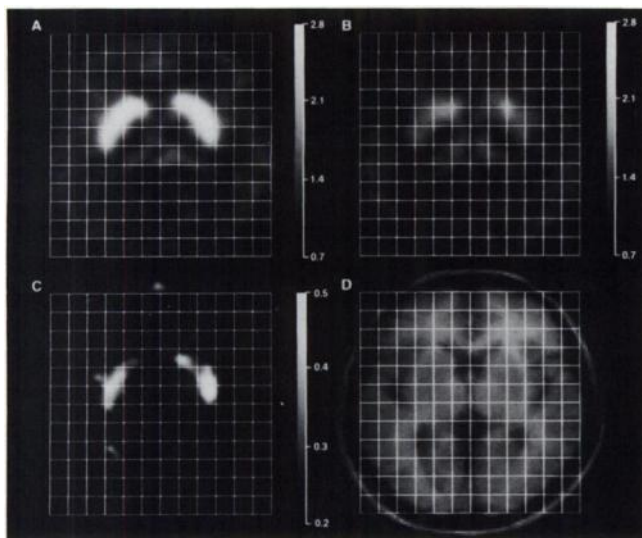
FIGURE 2. The pixel value-to-mean occipital radioactivity ratio images of individual subjects are first transformed into a common streotaxic space of the atlas of Talairach and Tournoux (24) and rescaled so that the length of the transverse and sagittal axes are equal to each other (15). (A) The averaged pixel radioactivity images for control subjects and Parkinson's disease patients (B). (C) The relative change image was calculated as in Figure 2A minus Figure 2B, normalized to Figure 2A. (D) The averaged MR image at 3.7 mm above the AC-PC plane, the level of the averaged PET images.

disease in vivo with the posterior half of putamen being most severely affected. A similar subregional posterior-to-anterior gradient was reported previously by Leenders et al. (9) using the influx constant of FDOPA which "includes effective blood-to-brain transport and specific processing of the tracer by the tissue." The following points are unique to the present study. First, the present FDOPA-PET method yielded direct measurements of both the relative DDC activity and the unidirectional blood-to-brain clearance. Second, we improved the anatomical identification of the cortical regions and striatal subdivisions by mapping of correlated MRI/PET volumetric data onto a standarized stereotaxic coordinate space.

The constraints of the present method were derived from the theoretical and practical observation that the two steps of tracer FDOPA metabolism in brain, namely the transport across the BBB (26), and the enzymatic conversion to fluorodopamine, are both governed by Michaelis-Menten kinetics (22). First, we constrained the transport ratio between OMFD and FDOPA, the main metabolite of peripheral origin and competitor for the large neutral amino acid transport, to 2.3 (21). Second, we constrained the tracer partition volume of striatal subdivisions to the individual's estimate of the frontal cortex (23). The constraints had two advantages; circulation time for data analysis could be limited to 40 min during which the loss of fluorodopamine metabolites from brain is likely to be negligible, and they yielded accurate estimates in smaller structures such as the caudate head and subdivisions of the putamen. In a previously published article, we compared analytical methods of

FDOPA study including the k_3^D coefficient used in the present study and by Huang et al. (27), the slopes of graphical analyses normalized to plasma FDOPA activity (6) or to the radioactivity of a reference region (7,8), and the simple striato-to-occipital activity ratio (28). We found the present method one of the most powerful in discriminating between normal and pathological FDOPA kinetics in striatum of patients with Parkinson's disease (12). In the present study, we observed no overlap in the k_3^D values of the posterior putamen of control subjects and Parkinson's disease patients. In the anterior putamen only one k_3^D value of a Parkinson's disease patient fell within the normal range. Brooks et al. and Sawle et al. also reported similarly good discrimination between the two groups in putamen by means of the uptake constant (7,11).

Biochemical studies of postmortem brain revealed a large variation of the normal striatal DDC activity both among reports and within individual reports (the coefficients of variation of 30%–60%) (29–32), probably due to the variable duration between death and examination, affecting the stability of the enzyme (30). The changes of the striatal DDC activity in Parkinson's disease also vary significantly among reports from 4.4% (29) to 44.5% (31) of the control value for putamen. Agid et al. (33) reported reductions of DDC activity to 45% of the control value in caudate nucleus and to 25% in putamen as the mean of the literature values. Thus, the present method yielded values for the reduction in relative DDC activity comparable to values in vitro. The magnitude of reductions observed postmortem are slightly greater than the present observations in vivo, perhaps due to different stages of the disease.

Quantitatively, observations made with FDOPA and PET indicate a reduction of the k_3^D or the uptake constants to 40% of the normal values in patients with moderately severe Parkinson's disease. In contrast, postmortem assays indicate a strikingly severe reduction of striatal dopamine content to around 10% of the normal value (34). This severe depletion of dopamine relative to a modest reduction of the DDC activity remains to be studied in the future. As possible explanations for the discrepancy, we have proposed a competition between decaboxylation and efflux of L-DOPA to the circulation (16). We also demonstrated increased dopamine turnover and reduced retention of dopamine in Parkinson's disease (35).

We found no significant change of the unidirectional blood-to-brain clearance of FDOPA in Parkinson's disease. In MPTP-treated monkeys, the results are controversial. Alexander et al. (13), using a microdialysis technique, reported a significant reduction of the blood-to-brain transport of levodopa, while data from Doudet et al. (36) suggested no change of the transport of OMFD. Our findings may be further confirmed by using tracers specific to the large neutral amino acids such as OMFD and [^{11}C]-aminocyclohexancarboxylate (37,38). According to Crone's equation, the K_1 coefficient is a function of cerebral blood flow and of the permeability-surface area product (39). Leenders et al. (9) reported no significant change of cere-

bral blood flow in the caudate and putamen of Parkinson's disease patients. This finding along with our own results suggest no pathological changes in density and function of large neutral amino acid transport in Parkinson's disease. The rate of dopamine synthesis from exogenous, therapeutic levodopa can be calculated as $C_a K^D$, where C_a is the concentration of levodopa in plasma and K^D the net clearance of FDOPA, analogous to measurements of cerebral glucose utilization. K^D is given by $K_1^D k_3^D / [k_2^D + k_3^D]$, where k_2^D is the fractional brain-blood clearance. Therefore, impairment of BBB transport, were it present, would diminish levodopa delivery to striatum and also subsequent dopamine production.

Interestingly, the caudate K_1^D values of the present study were 70%~82% of putamen values. Koeppe et al. (38) reported that the caudate K_1 values of [^{11}C]-aminocyclohexancarboxylate were 72% of the putamen values in normal subjects. In addition, Leenders et al. (9) found regional blood flow values of caudate were 83%~84% of the putamen values in both normal subjects and Parkinson's disease patients. This quantitative agreement supports a successful separation of blood-to-brain transport and DDC activity in the present method.

The striatal-to-occipital radioactivity ratio is an index of FDOPA uptake by the striatum (28). The ratio significantly correlated with the DDC activity for normal subjects and for Parkinson's disease patients (12). Maps of this index ([pixel-occipital]/occipital) have been used to detect postoperative changes in FDOPA uptake in Parkinson's disease patients who received transplantation of fetal dopamine neurons (40). We transformed such ratio images to a common stereotaxic coordinate space and averaged across subjects of the same clinical category to present a pattern of FDOPA accumulation common to the disease (16). Such averaged images can provide a characteristic pattern of biological variables associated with diseases. In this study, we also provided a map of changes in FDOPA uptake and metabolism common to the present patient group. Thus, we propose that FDOPA, in analogy to cerebral activation studies, can be used as a clinical tool for identifying an abnormality of biological variables in clinical groups as compared to normal subjects.

CONCLUSION

The relative DDC activity was differentially reduced in subdivisions of the striatum in Parkinson's disease while the blood-to-brain transport of large neutral amino acids remained unchanged. PET imaging was useful in demonstrating changes of FDOPA accumulation in Parkinson's disease.

ACKNOWLEDGMENTS

REFERENCES

1. Aquilonius S-M, Långström B, Tedroff J. Brain dopaminergic mechanisms in Parkinson's disease evaluated by positron emission tomography. *Acta Neurol Scand* 1989;126:55–59.
2. Eidelberg D. Positron emission tomography studies in parkinsonism. *Neurologic Clinics* 1992;10:421–433.
3. Calne DB, Snow BJ. PET imaging in Parkinsonism. *Adv Neurol* 1993;60:484–487.
4. Patlak CS, Blasberg RG, Fenstermacher JD. Graphical evaluation of blood-to-brain transfer constants from multiple-time uptake data. *J Cereb Blood Flow Metab* 1983;3:1–7.
5. Patlak CS, Blasberg RG. Graphical evaluation of blood-to-brain transfer constants from multiple-time uptake data: generalization. *J Cereb Blood Flow Metab* 1985;5:584–590.
6. Martin WPW, Palmer MR, Patlak CS, Calne DB. Nigrostiriatal function in humans studied with positron emission tomography. *Ann Neurol* 1989;26:535–542.
7. Brooks DJ, Ibanez V, Sawle GV, et al. Differing patterns of striatal ^{18}F-dopa uptake in Parkinson's disease, multiple system atrophy, and progressive supranuclear palsy *Ann Neurol* 1990;28:547–555.
8. Hartvig P, Agren H, Reibring L, Tedroff J, Bjurling P, Kihlberg T. Brain kinetics of L-[β-^{11}C] DOPA in humans studied by positron emission tomography. *J Neural Transm* 1991;86:25–41.
9. Leenders KL, Salmon EP, Tyrrell P, et al. The nigrostriatal dopaminergic system assessed in vivo by positron emission tomography in healthy volunteer subjects and patients with Parkinson's disease. *Arch Neurol* 1990;47:1290–1298.
10. Snow BJ, Peppard RF, Guttman M, et al. Positron emission tomographic scanning demonstrates a presynaptic dopaminergic lesion in Lytico-Bodig. The amyotrophic lateral sclerosis-parkinsonism-dementia complex of Guam. *Arch Neurol* 1990;47:870–874.
11. Sawle GV, Playford ED, Burn DJ, Cunningham VJ, Brooks DJ. Separating Parkinson's disease from normality. Discriminant function analysis of fluorodopa F-18 positron emission tomogrphy data. *Arch Neurol* 1994;51:237–243.
12. Hoshi H, Kuwabara H, Léger G, Cumming P, Guttman M, Gjedde A. 6-[^{18}F]fluoro-L-DOPA metabolism in living human brain: a comparison of six analytical methods. *J Cereb Blood Flow Metab* 1993;13:57–69.
13. Alexander GM, Schwartzman RJ, Grothusen JR, Gordon SW. Effect of plasma levels of large neutral amino acids and degree of parkinsonism on the blood-to-brain transport of levodopa in naive and MPTP parkinsonian monkeys. *Neurology* 1994;44:1491–1499.
14. Guttman M, Leger G, Cedarbaum JM, et al. 3-O-methyldopa administration does not alter fluorodopa transport into the brain. *Ann Neurol* 1992;31:638–643.
15. Evans AC, Marrett S, Neelin P, et al. Anatomical mapping of functional activation in stereotaxic coordinate space. *Neuro-Image* 1992;1:43–63.
16. Gjedde A, Léger G, Cumming P, et al. Striatal L-dopa decarboxylase activity in Parkinson's disease in vivo: implications for the regulation of dopamine synthesis. *J Neurochem* 1993;61:1538–1541.
17. Hoehn MM, Yahr MD. Parkinsonism: onset, progression and mortality. *Neurology* 1967;17:427–442.
18. Evans AC, Thompson CJ, Marret S, et al. Performance characteristics of the PC-2048: a new 15-slice encoded-crystal PET scanner for neurological studies. *IEEE Trans Nucl Sci* 1991;35:730.
19. Cumming P, Léger G, Kuwabara H, Gjedde A. Pharmacokinetics of plasma 6-[^{18}F]fluoro-L-3,4-dihydroxyphenylalanine ([^{18}F]FDOPA) in humans. *J Cereb Blood Flow Metab* 1993;13:668–675.
20. Evans AC, Marrett S, Torrescorzo J, Ku S, Collins L. MRI-PET correlative analysis using a volume of interest (VOI) atlas. *J Cereb Blood Flow Metab* 1991;11:A69–A78.
21. Reith J, Gjedde A, Kuwabara H, et al. Blood-brain transfer and metabolism of 6-[^{18}F]fluoro-L-DOPA in rat. *J Cereb Blood Flow Metab* 1990;10:707–719.
22. Gjedde A, Reith J, Dyve S, et al. Dopa decarboxylase activity of the living human brain. *Proc Natl Acad Sci USA* 1991;88:2721–2725.
23. Kuwabara H, Cumming P, Reith J, et al. Human striatal L-DOPA decarboxylase activity in vivo using 6-[^{18}F]fluoro-DOPA and positron emission tomography: error analysis and application to normal subjects. *J Cereb Blood Flow Metab* 1993;13:43–56.
24. Talairach J, Tournoux P. *Co-planar stereotaxic atlas of the human brain.*

Three-dimensional proportional system: an approach to cerebral imaging (Rayport M, trans), New York: Thieme Medical; 1988.

25. Cupples LA, Heeren T, Schatzkin A, Colon T. Multiple testing of hypotheses in comparing two groups. *Ann Int Med* 1984;100:122–129.

26. Oldendorf WH, Szabo J. Amino acid assignment to one of three blood-brain barrier amino acid carriers. *Am J Physiol* 1976;230:94–98.

27. Huang S-C, Yu D-C, Barrio JR, et al. Kinetics and modeling of L-6-[^{18}F]Fluoro-sc dopa in human positron emission tomographic studies. *J Cereb Blood Flow Metab* 1991;11:898–913.

28. Leenders KL, Palmer AJ, Quinn N, et al. Brain dopamine metabolism in patients with Parkinson's disease measured with positron emission tomography. *J Neurol Neurosurg Psychiatry* 1986;49:853–860.

29. Lloyd L, Hornykiewicz O. Parkinson's disease: activity of L-dopa decarboxylase in discrete brain regions. *Science* 1970;170:1212–1213.

30. MacKay AVP, Davies P, Dewar AJ, Yates CM. Regional distribution of enzymes associated with neurotransmission by monoamines, acetylcholine and GABA in the human brain. *J Neurochem* 1978;30:827–839.

31. Nagatsu T, Kato T, Numata Y, et al. Phenylethanolamine *N*-methyltransferase and other enzymes of catecholamine metabolism in human brain. *Clin Chim Acta* 1977;75:221–232.

32. Rinne UK, Sonninew V, Laaksonen H. Responses of brain neurochemistry to levodopa treatment in Parkinson's disease. *Adv Neurol* 1979;24:259–274.

33. Agid Y, Javoy-Agid F, Ruberg M. Biochemistry of neurotransmitters in Parkinson's disease. In: Marsden CD, Fahn S, eds. *Movement disorders,* vol. 2. London: Butterworths 1987:166–230.

34. Hornykiewicz O, Kish SJ. Biochemical pathophysiology of Parkinson's disease. *Adv Neurol* 1986;45:19–34.

35. Kuwabara H, Cumming P, Léger G, et al. Metabolism of 6-[F-18]fluorodopamine is enhanced in patients with parkinson's disease [Advances]. *J Nucl Med* 1993;34:31P.

36. Doudet DJ, Miyake H, Finn RT, et al. 6-^{18}F-L-DOPA imaging of the dopamine neostriatal system in normal and clinically normal MPTP-treated rhesus monkeys. *Exp Brain Res* 198;78:69–80.

37. Wahl L, Chirakal R, Firnau G, Garnett ES, Nahmias C. The distribution and kinetics of [^{18}F]6-fluoro-3-O-methyl-L-dopa in the human brain. *J Cereb Blood Flow Metab* 1994;14:664–670.

38. Koeppe RA, Mangner T, Betz AL, et al. Use of [^{11}C]aminocyclohexanecaboxylate for the measurement of amino acid uptake and distribution volume in human brain. *J Cereb Blood Flow Metab* 1990;10:727–739.

39. Crone C. The permeability of capillaries in various organs as determined by the use of the "indicator diffusion" method. *Acta Physiol Scand* 1963;58:292–305.

40. Sawle GV, Bloomfield PM, Björklund A, et al. Transplantation of fetal dopamine neurons in Parkinson's disease: PET [^{18}F]6-L-fluorodopa studies in two patients with putaminal implants. *Ann Neurol* 1992;31:166–173.